Supergene nickel ore deposits controlled by gravity-driven faulting and slope failure (Peridotite Nappe, New Caledonia)

Marion Iseppi, Brice Sevin, Dominique Cluzel, Pierre Maurizot, Benjamin Le Bayon

Supergene nickel ore deposits controlled by gravity-driven faulting and slope failure (Peridotite Nappe, New Caledonia)

Marion Iseppi [1, 2]*, Brice Sevin [2], Dominique Cluzel [1], Pierre Maurizot [2] and Benjamin Le Bayon [3]

[1] Institute of Exact and Applied Sciences (ISEA), Université de la Nouvelle-Calédonie, Avenue James Cook, Nouméa, New Caledonia

[2] Geological Survey of New Caledonia, DIMENC, 1 ter Rue Unger, Nouméa, New Caledonia

[3] French Geological Survey, BRGM, 3 Avenue Claude Guillemin, Orléans, France

* marion.iseppi@univ-nc.nc

Abstract

New Caledonia holds one of the largest supergene nickel ore deposits worldwide. Two main ore types are recognized: i) oxide and ii) hydrous Mg silicate types. Our study focuses on the latter type, usually located in elevated parts of the Peridotite Nappe, forming the so-called plateau and slope deposits. Understanding the controls of these ore deposits is important in regard to sustainability of nickel mines; however, to date there are only a few models to refer to, and structural aspects have been generally underestimated.

From its formation at a spreading ridge to Eocene obduction, the Peridotite Nappe of New Caledonia underwent several episodes of brittle fracture that mostly preceded weathering. We suggest that inherited fractures coated with serpentine “polymorphs” play a major role in the Ni enrichment process. Fracture analysis shows that this early fracture network share the same orientations with lineaments of peridotite massifs and controlled erosion and plateau dissection during uplift events. The subsequent steep slopes together with circulating waters within serpentinized fractures parallel to underlying valleys lead to slope failure. The collapse of plateau edges provoked plateau decompression and hence multi-directional extension. Gravity-driven faulting caused preferential opening of joints within the hanging walls of faults. The lateral permeability contrast favored preferential weathering and eventually resulted in an increase of Ni content in the saprock. The controlling faults have a specific polyphase infill, which could be a metallotect and a potential guide for nickel exploration.

Introduction

New Caledonia holds about 8% of nickel global reserves and ranks fifth among World's nickel ore producers (U.S. Geological Survey, 2017). Nickel ore was formed by tropical weathering of peridotite and is hosted at the base of the weathering profile. Exploration of this type of deposits requires a very dense and expensive drilling pattern due to the high variability of the thickness and grade of the nickel-bearing level.

One third of New Caledonia is covered by ultramafic rocks which underwent weathering since the late Eocene. From base to top, the weathering profile is composed of a saprock or saprolite horizon, a limonitic horizon and a ferricrete at the top. Supergene nickel ore deposits correspond to the hydrous Mg-Ni silicate-type ore and oxide-type ore respectively, depending upon the main nickel-bearing mineral phase. These ores are mined within the saprock/saprolite and at the base of the limonite horizon respectively (Brand et al., 1998; Freyssinet, 2005; Butt and Cluzel, 2013).

In New Caledonia, ore-forming processes resulting in nickel supergene deposits were not extensively studied until the 2000s due to multiple factors such as abundance of the resource, easy open-cast mining, and complexity of geological controls. However, two main contributions based on the classic *per descensum* model should be mentioned; Trescases (1973), in a geochemical and geomorphological approach, assessed the balance between weathering and erosion during uplift and subsidence, and Leguéré (1976) was the first to point out the prominent control of the fracture network on Ni mineralization.

Understanding the controls of supergene deposits is crucial in regard to sustainability of nickel mines; but, to date there are only a few models to refer to, and mainly targeted to specific deposits.

Genna et al. (2005) proposed a model based chiefly on karst-like land forming. Accordingly, sinkholes are associated with landslide-like structures limited at the base by 'listric' faults, in which hydrous Ni silicate ore is concentrated. As a consequence, the discontinuities that controlled nickel concentration were not inherited from basement fractures, but neo-formed as a direct consequence of the weathering process.

Cluzel and Vigier (2008) highlighted the synkinematic character of some garnierite crack seals, and suggested that active faulting was associated with newly formed Mg-Ni silicate ore. In addition, they also described polyphase supergene infill of early serpentine-coated faults rooted in the bedrock, thus suggesting some influence of the pre-existing fracture network. The changing nature of infill, from garnierite to silica and finally Fe oxyhydroxides, is considered as a record of the downward migration of the weathering front through time.

Cathelineau et al. (2016a) mentioned the strong influence of the inherited fracture network, which is almost systematically reused by supergene infill. Although they report only few evidences of synkinematic character of Ni silicate veins, the presence of hydraulic breccia and preferred orientation of Ni silicate veins indicate some tectonic control. On the basis of paleotemperature estimates of quartz formation, ranging from 50°C to 95°C (Quesnel et al., 2016), Cathelineau et al. (2016a) proposed an alternative 'hydrothermal' model of Ni concentration. Accordingly, meteoric water infiltrated from the surface, was slightly heated at depth and then advected within the peridotites; a process previously proposed by Guillou-Frottier et al. (2015).

Fritsch et al. (2016), through a mainly mineralogical approach, described a systematic superimposition of hydrous Mg-Ni silicates on the serpentine-bearing fractures. Authors also argue that meteoric water infiltrating the peridotites would have interacted with a low-temperature hydrothermal field following the cooling of the Peridotite Nappe.

More recently, Quesnel et al. (2017) have evidenced lateral transfer of Ni, on the basis of geochemical data from drill-cores of the Koniambo deposit. Accordingly, Ni was transferred downslope from now-eroded topographic highs within the water table of the saprock.

Almost all above mentioned models are based upon specialists views (geomorphology, mineralogy, geochemistry, and structural geology), while an integrated approach is still missing.

The pragmatic guidelines commonly used by mining geologists are worth taking into consideration. In their experience, nickel mineralization is correlated with the serpentinization degree and density of the fracture network (Orloff, 1968; Pelletier, 1996; Trotet et al., 2014). The role of fractures, either passive (*per descensum* conduits in a static environment) or dynamic (fault motion with hydraulic brecciating and crack seal) has been highlighted by some authors, but on the whole, the importance of the inherited fracture network in the control of Ni deposits has been minored, and, with some exceptions, tectonic aspects have been overlooked.

In this paper we propose a refined new model based on structural analysis in several mining areas and DEM analysis that may apply to most silicate-type supergene nickel deposits of New Caledonia.

Geological setting

Peridotite Nappe

New Caledonia is located in the Southwest Pacific where it forms the emerged northern part of the Norfolk Ridge, a continental ribbon rifted from Eastern Gondwana in the late Cretaceous (Hayes and Ringis, 1973) (Fig. 1A). The Peridotite Nappe (Avias, 1967) is a major litho-tectonic unit obducted in late Eocene time over a substratum composed of several sedimentary and metamorphic units

(Paris, 1981; Aitchison et al., 1995; Cluzel et al., 2001). Ultramafic rocks entirely cover the southeastern part of the main island, termed 'Massif du Sud', and crop out in a series of tectonic klippes aligned along the west coast (Fig. 1B).

The Peridotite Nappe was emplaced by obduction of the oceanic mantle lithosphere of the Loyalty Basin (Collot, 1987), which corresponds to the eastern part of a larger marginal basin of possible Late Cretaceous age (Aitchison et al., 1995; Cluzel et al., 2001). This basin was inverted and transformed in a fore-arc during the Eocene (Aitchison et al., 1995; Cluzel et al., 2001; Milsom, 2003; Edwards et al., 2015). The northeast-dipping subduction that eventually led to obduction started near the ridge and involved young and hot lithosphere (Ulrich et al., 2010). Subduction inception is time-constrained at ca. 56 Ma by high-temperature amphibolites of the metamorphic sole (Cluzel et al., 2012). Obduction occurred after the latest Eocene, age of the youngest sediments overthrust by the Peridotite Nappe (Cluzel et al., 1998; Maurizot and Cluzel, 2014) and before the Late Oligocene, age of crosscutting granitoids (Paquette and Cluzel, 2007).

The Peridotite Nappe is mainly composed of extremely refractory harzburgites and dunites with minor lherzolites (Prinzhofer, 1981; Ulrich, 2010), the latter being mainly located in northern klippes. Peridotites commonly display a compositional layering of alternating harzburgite and dunite (Guillon, 1975; Prinzhofer, 1981).

The driving mechanism of obduction remains a matter of debate and contrasting models have been proposed: i) blocked subduction (Aitchison et al., 1995; Cluzel et al., 2001); ii) 'push from the rear' mechanism driven by back-arc basin opening (Gautier et al., 2016); or alternatively, iii) "passive obduction", e.g., gravity-driven emplacement triggered by the exhumation of HP-LT rocks (Lagabrielle and Chauvet, 2008; Lagabrielle et al., 2013).

Regardless of the mechanism, obduction occurred during a period of warm climate and peridotites were probably weathered soon after emersion. The serpentinite basal 'sole' contains syn-tectonic magnesite veins of supergene origin, which suggest that the Peridotite Nappe probably underwent weathering during the last stages of obduction (Quesnel et al., 2013). Pre- Miocene weathering and erosion of the Peridotite Nappe is recorded by lateritic detritism in Early Miocene sediments (Coudray, 1976), and dated by paleomagnetism of in situ ferricrete (Sevin et al., 2012; Maurizot et al., 2016).

Early fracturation and serpentinization

Fracturation and serpentinization are major features, which are known to control weathering by allowing water circulation, and nickel enrichment through the formation of supergene silicate ore (Golightly, 1981; Pelletier, 1996; Butt and Cluzel, 2013).

From spreading to obduction, the peridotites have undergone several episodes of cooling, hydration, and deformation that resulted in the formation of minerals of the serpentine group at the expense of olivine and orthopyroxene (Orloff, 1968; Ulrich et al., 2010). The degree of serpentinization is highly variable and can be pervasive, or alternatively, restricted to veins and fracture walls (Dilek et al., 1997; Andreani et al., 2007; Rouméjon and Cannat, 2014; Rouméjon et al., 2015). Different types of serpentine mineralization are observed: i) diffuse intragranular serpentinization; ii) a network of cm-thick and several m-long joints and faults with serpentinized walls; and, iii) a thick serpentinite mylonite sole at the base of the Peridotite Nappe. Only the first two types, which play a prominent role in supergene nickel enrichment, will be considered here.

The diffuse serpentinization consists of a thin mesh developed in olivine cracks usually filled by lizardite. It is commonly randomly oriented and likely formed in static conditions (Evans et al., 2013; Frost et al., 2013; Fritsch et al., 2016).

Joints and faults form a dense, complex and polyphase fracture network, which bears various minerals of the serpentine family, namely lizardite, antigorite, chrysotile and polygonal serpentine (Lahondère et al., 2010; Ulrich, 2010; Quesnel, 2015; Cathelineau et al., 2016a). Crystallization of serpentine "polymorphs" depends on many parameters (fluid composition and saturation, surface of reaction, fluid and lithospheric pressure, etc.) and "polymorphs" can form in a large range of pressure and temperature (Andreani, 2003; Evans, 2004; Schwartz et al., 2013; Guillot et al., 2015). Lizardite, chrysotile and polygonal serpentine are known to be stable at temperatures up to 300°C and at low to very low pressure (Evans, 2004; Andreani et al., 2008; Schwartz et al., 2013; Guillot et al., 2015).

In the Peridotite Nappe, the serpentine-bearing fracture network usually shows a N130°E dominant trend, locally associated with subordinate N090°E, N045°E and N000°E directions (Leguéré, 1976; Moutte and Paris, 1976; Robineau et al., 2007; Jeanpert et al., 2016). These directions are also recognizable as lineaments at island scale (Fig. 1B).

Weathering and Ni-enrichment of peridotites

Weathering of ultramafic rocks is promoted by warm and wet tropical climate, leading to peridotite dissolution and karst-like landforms (Wirthmann, 1965; Trescases, 1973; Latham, 1986; Genna et al., 2005). Weathering of peridotite leaves a considerable residue, which constitutes a thick lateritic regolith (Avias, 1969; Trescases, 1973; Latham, 1986). Infiltration of meteoric water in otherwise impermeable fresh peridotite is enabled by the fracture network (Chételat, 1947; Trescases, 1973; Leguéré, 1976; Genna et al., 2005; Join et al., 2005). Hydrolysis of Fe-Mg silicates (olivine, orthopyroxene and serpentine) allows leaching of Mg and Si while less mobile elements (Fe,

Mn, Cr, Ni and Co) remain in residual minerals (chromite) or recombine into newly formed mineral phases (hydrous Mg silicates, Fe oxyhydroxides, Mn- or Co-oxides, etc.). Nickel released by the dissolution of olivine can be incorporated inside the lattice or partly adsorbed at the surface of serpentine (Trescases, 1973; Pelletier, 1996).

Typically, the weathering profile in New Caledonia is composed from base to top of four horizons (Eggleton, 2001; Deraisme et al., 2014) (Fig. 2):

i) Saprolite formed of fractured and partly weathered peridotite, called saprock when there is less than 20% weathering;

ii) Yellow limonite, in which parent rock texture is still recognizable but considerably flattened;

iii) Red limonite, in which texture disappears, and where goethite is progressively replaced by hematite;

iv) Granular (pisolithic) horizon and indurated ferricrete capping the profile.

Horizons i) and ii) contains the main Ni mineralizations and depending upon the relative amount of saprolite/saprock and yellow limonite, form two distinct ore types that may coexist in one single deposit. The saprock hosts the hydrous Ni-Mg silicate ore type, whilst yellow limonite hosts the oxide type ore (Troly, 1979; Golightly, 1981; Pelletier, 1996; Freyssinet, 2005; Butt and Cluzel, 2013; Maurizot et al., in press.). In the hydrous Ni-Mg silicate ore, nickel leached from peridotite recombines with Si and Mg to form a mixture of poorly crystallized silicate of the serpentine, talc or sepiolite group, to which should be added chlorite and smectite groups (Fritsch et al., 2016). The Ni-dominated silicate, first discovered in New Caledonia by J. Garnier (1867) is termed garnierite (Liversidge, 1880), whilst the Mg dominated silicate is referred to as deweylite (Bish and Brindley, 1978). Both species preferentially precipitate in open spaces, as crack seals and fracture films (Cathelineau et al., 2016b) in the saprock. In the oxide ore, nickel can be incorporated in substitution to iron or adsorbed by goethite minerals in the limonite horizon (Trescases, 1973). Nickel content in the red limonites and ferricrete on top of the weathering profile is not economic at present, they are considered as waste.

In New Caledonia, the two ore types coexist in most deposits but silicate ore is dominant in west coast klippes and elevated areas of the northern part of Massif du Sud, while oxide type forms large ore deposits in low lands of the Massif du Sud (Maurizot et al., in press.).

The interaction of weathering and fracture network leads to high variability of bedrock morphology and thickness of the weathering profiles, and to overall complexity of orebodies (Trescases, 1973; Genna et al., 2005; Deraisme et al., 2014).

196 *Geomorphology of the Peridotite Nappe*

197 Combination of uplift and erosion (Freyssinet, 2005; Chevillotte et al., 2006; Chardon et al., 2008)
198 during a period of climate warming (Lower Oligocene Warm Event and mid-Miocene Climatic
199 Optimum) enhanced by the northward migration of the Australian Plate (Zachos et al., 2001; Zachos
200 et al., 2008; Sevin et al., 2014), resulted in different types of morphology which likely correspond to
201 steps in a continuum (Fig. 1B):

202 i) Low-elevated areas with flat surfaces are well developed in the south of Massif du Sud
203 (Trescases, 1973; Chevillotte et al., 2006);

204 ii) Plateaus, which are morphologically inverted lowlands, are mainly exposed in the
205 northernmost klippes (Bélep, Tiébaghi, Poum) (Latham, 1986);

206 iii) Partly dissected plateaus with stepped planation surfaces and incised glacis, e.g.
207 Koniambo and Boulinda massifs (Latham, 1986);

208 High-elevated, dissected, and mountainous massifs where weathering surfaces are
209 restricted to slopes such as the Mé Maoya Massif.

210

211 **Methodology**

212 *Field methodology*

213 Peridotites are generally covered by a thick regolith, which prevents observation of structures.
214 Therefore, the field study focused on natural cliffs and open-pit mines where saprock and bedrock
215 are best exposed. Fourteen sites have been visited ('grey stars', Fig. 1B) and 520 faults and joints
216 were measured.

217 In the southern part of the island, the 200m-high cap N'Dua cliffs, which correspond to the
218 uplifted NW side of a major fault (Lagabrielle et al., 2005), show good rock exposures allowing
219 fracture analysis on top and at the base of the cliffs (Fig. 3).

220 In mining sites, the field study focused on both plateau and slope deposits (Bailly et al., 2014) in
221 order to compare the structures associated with each type. An exhaustive survey of fractures and
222 their infills/coatings has been undertaken at each site. The results of two representative mine sites
223 are presented:

224 i) The Kopéto Massif (Fig. 1B), on which six open-pit mines operating plateau and slope
225 deposits have been studied ('Exploitation', Fig. 4A). In the northeastern part of Kopéto,
226 special attention has been given to the Vieille Carrière site located at 800 m asl;

ii) In the north of Boulinda Massif, the Trafalgar site is a slope deposit, which overlooks the river valley oriented N050°E that crosscuts the massif.

A focus has been made on the geometry and kinematics of slickensided faults with supergene mineral coatings, thereafter called supergene faults.

A distinction has been made between the central fault core or slip surface and the surrounding volume of brittlely deformed wallrock mechanically related to the growth of the fault zone, known as the fault damage zone (Sibson, 1977; Chester and Logan, 1986; Peacock et al., 2000).

Lineament analysis

This field survey was combined with a lineament analysis from a 10 meter digital elevation model (DEM) (DTSI, 2013). In the context of this study, the lineament analysis attempts to distinguish those lineaments which are adapted to underlying structures from those associated with downslope runoff and erosion. The analysis was carried out in the weathered horizon topping the massif and lineaments were drawn where their direction was clearly independent from the direction of the main slope line. Lineaments following the main slope line are organized in a radial pattern, while lineaments adapted to underlying structures extend over erosional features such as crests and rivers.

Results

Fracture typology

At outcrop scale, fractures may be distinguished on the basis of their coatings or infills. As previously stated, two types of infills/coatings are commonly associated with fractures: primary serpentines and supergene minerals.

The four serpentine “polymorphs” have been determined in New Caledonia within fractures of the saprock and bedrock by Raman spectroscopy and others technics (Ulrich, 2010; Quesnel et al. 2016). Because the early serpentinization is not the main subject of this paper, serpentine coatings and infills are hereafter simply being termed ‘serpentine’.

Three types of supergene silicates may be distinguished: garnierite, deweylite and silica. Silica systematically postdates garnierite and deweylite (Cluzel and Vigier, 2008; Cathelineau et al., 2016a; Fritsch et al., 2016). These supergene infills are found in faults, joints and as matrix or cement in breccia.

Observations in extraction zones show that the primary fracture network of the protolith and supergene infills are closely associated. The progressive downward weathering used these pre-existing discontinuities as preferential circulation conduits inducing differential weathering.

Bedrock fracture network

The fresh rock exposures of cap N'Dua cliffs allow a good appraisal of the geometry of the fracture network in the unweathered bedrock. These fractures are coated with serpentine with no supergene coating or infill. The fracture network shows directions N000-020°E, N050-070°E, N090-100°E and N120-140°E with variable dips from 20 to 90° (Fig. 3A). Sets of fractures exhibit variable spacing from a few tens to hundreds of metres, proportional to their length, and cross-cut each other forming dihedral geometry (Fig. 3B). Fracture spacing is constant from base to top and does not increase upward. It is noteworthy that serpentine-coated fractures within the bedrock show the same trends as the ones recognized at island scale.

Distribution of fractures in plateau deposits

Rectilinear segments of most ridges and valleys incising the peridotite massifs are an expression of the main structural directions at the island scale. The Kopéto Massif is crosscut by deep valleys oriented N010°E, N130°E, N050°E and N090°E (Fig. 4A). However, a partly dissected plateau covered by uneven regolith is preserved at an altitude of 1000 m, hosting several orebodies. The plateau is elongated along an E-W direction and lineament analysis from 10 m DEM (DTSI, 2013) shows directions similar to peripheral ridges and valleys (Fig. 4A). Orebodies are elongated, controlled to the north and south by N120°E and N090°E lineaments and subordinate N050°E lineaments (Kermes, Fig. 4A).

Most of the fracture network is coated by primary serpentine "polymorphs" indicating their belonging to an inherited fracture field. Fracture analysis shows that these serpentine-coated fractures have the same orientation as the main lineaments ('Serpentine fracture', Fig. 4A). But, only fractures conveniently oriented with respect to the plateau edges are reactivated. Reuse of ancient fractures resulted in precipitation of supergene minerals. A prime example is the northern part of the open pit Kermes where serpentine fractures are mainly oriented N020°E and N120°E, while supergene materials are only present in the latter orientation which also limits plateau edges (Fig. 4A).

Besides, geoelectrical imaging of the regolith, undertaken in the plateau of Tiébaghi (Fig. 1B) (Robineau et al., 2007), confirmed the thickening of the weathering profile in burrows controlled by similar supergene faults.

Distribution of fractures in slope deposits

Slope deposits are arranged in a radial pattern along plateau edges. These are usually controlled by a fracture parallel to the underlying valley while the other sets have subordinate role. On the northeastern side of Kopéto Massif, the pit Vieille Carrière is bounded to the northwest by a crest oriented N060°E. The serpentine fracture network shows various orientations but the pit is controlled by a supergene fault N060°E 35°SE reusing a large serpentine fault plane on the northern side of the pit parallel to the crest and the underlying ravine (Fig. 4A).

In this entirely excavated quarry, an exhaustive structural survey has been undertaken (Fig. 4B). Serpentinized fractures and those filled with supergene material as well, display N020°E, N090°E and N130°E average directions. About 70% of the fractures filled with supergene material display serpentinized walls indicating a reopening of inherited fractures (black dashed line, Fig. 4B). The remaining 30% are mainly several cm spaced joints filled with amorphous supergene minerals only; they are generally located in the hanging wall of the main supergene fault.

The exploration site Trafalagar (Fig. 5A) shows the morphology of a slope deposit in a pre-exploitation stage. The deposit is bound by a hm-scale fault coated by silica. This fault controls a large slump morphologically recognizable by its detachment scarp and the convex shape of the slipped mass (Fig. 5B). Figure 5C shows an equivalent structure that crops out in a creek oriented E-W. The fault is oriented N050°E 50°NW parallel to the underlying valley and shows a first dextral motion marked by slickensided serpentine, followed by dip-slip motion marked by striated supergene silica. The surface of the weathering profile on top of the slipped mass (Fig. 5B) shows colluvionned elements of ferricrete in-situ, indicating a probable dismantlement of the former profile. It is noteworthy that these detachments are fossils and no recent detachments have been observed.

Supergene fault geometry and associated breccias

Open pit mines within slope deposits and plateau deposits are mainly controlled by faults with a zoned infill at centimeter-scale, which highlights their polyphase character. Indeed, the zoning marked by various supergene minerals reveals that pre-existing fractures filled by older (higher temperature) serpentine minerals have been reactivated in supergene environment. Breccias associated to these faults have been described at cm-scale using six parameters: (1) fragment shape (angular to rounded), (2) size and distribution of fragments, (3) monomictic of polymictic nature, (4) presence of matrix or cement, (5) ratio between matrix (or cement) and fragments and (6) presence of voids and contact between fragments (Taylor and Pollard, 1993; Jébrak, 1997).

From the footwall to the hanging wall, the zoning consists of (Fig. 6):

- the footwall, which exhibits a dense serpentine-filled fracture network with no supergene coating or infill;

- a thick slickensided serpentine-coating, showing one or several motions;
- a clast-supported breccia 5 to 50 cm thick, composed of monogenic angular fragments of serpentine and serpentinized peridotite;
- a fault gouge a few cm thick, composed of breccia consisting of small rounded fragments of serpentine and serpentinized peridotite, imbedded in a matrix of various supergene material: brownish silica (Fig. 5C), deweylite (Fig. 7A) or garnierite (Fig. 7B);
- a fault 'mirror' commonly showing dip-slip striation. Occasional lenses of deweylite display sigmoidal duplex-like structure, which unambiguously indicate dip-slip motion;
- a clast-supported monomictic breccia several cm thick, composed of angular fragments in contact with each other and leaving open spaces, a characteristic feature of collapse breccia. The open spaces are partly filled with horizontally layered brownish amorphous silica (Fig. 7C) which possibly indicate a post-kinematic downward infill by silica gel (Kirkpatrick et al., 2013).
- the highly fractured hanging wall where open joints, 1 to 50 cm wide, have been partly cemented or coated by supergene material (Fig. 5C). Some veins are filled with brownish silica which contains cm-scale angular serpentine fragments extracted from the vein walls (Fig. 7D). These veins, which are absent from the footwall are likely due to hydro-fracturing during faulting.

Discussion

Structural analysis of already mined areas shows that the preexisting fracture network plays a prominent role in the formation of supergene nickel deposits not only by controlling water infiltration in a passive way but also by increasing fracture opening.

Serpentine-filled fractures play a double role as drain and screen. The serpentine infill of fractures seems more resilient to weathering than the peridotite host rock, and generally appear as residue in the limonite horizon (Trescases, 1973; Pelletier, 1996; Bailly et al., 2014; Sevin, 2014; Roqué-Rosell et al., 2016), which means that serpentine infill has a low permeability compared to the rest of the rock. Along steeply dipping fractures, the rock is weathered in a symmetrical fashion indicating that they played the role of a drain. In contrast, along gently dipping fractures, the weathering is more important on the hanging wall indicating that they played the role of a drain and a screen as well, preventing water to flow across the serpentinite coating (Bailly et al., 2014; Sevin, 2014).

The serpentine-filled (i.e. pre-weathering) fracture network yields the same orientations as the main lineaments determined by DEM analysis. These orientations closely correspond to valleys and ridges and hence to the bulk massif morphology (Fig. 1B, Fig. 3A and Fig. 4A). This morphology results from erosion of an older smooth surface probably during the early Miocene uplift described by Sevin

et al. (2014). The incision of the hydrographic network was guided by pre-existing faults and developed steep unstable slopes on massif edges.

On residual plateaus, the weathering profile is usually thicker than on flanks and several authors described the thickness of the weathering profile as an inverse function of slope (Maurizot et al., in press.; Chételat, 1947; Trescases, 1973; Avias, 1978). Furthermore, Quesnel et al. (2017) noted a general Ni- enrichment under thin limonite cover partially eroded or reworked on gentle slopes compared to topographic highs.

Slope collapse process is evidenced by the occurrence of normal faults upstream to slope deposits, which reuse serpentine-filled faults parallel to the direction of the underlying valleys (Fig. 3, Fig. 4 and Fig. 5) but also by space opening in the hanging wall of the fault (Fig. 6 and Fig. 7c). The occurrence of similar features on faults that control plateau deposits suggests a similar process.

These faults are systematically underlined by supergene matrix-supported breccias and hydraulic breccias in the hanging wall (Fig. 5C, Fig. 5D, Fig. 6 and Fig. 7B) in which the high matrix/element ratio indicated important dilation. Cathelineau et al. (2016a) interpret these breccias as a consequence of low temperature hypogene hydrothermal circulation. However, because these breccias are associated with newly formed supergene minerals (Fig. 7A and Fig. 7B) which are absent of the fresh bedrock, they rather result from supergene processes. In our interpretation, the important dilation exhibited by these breccias is probably due to fluid overpressure. The increase of fluid pressure within the fault resulted in rock failure, followed by sudden pressure drop afterwards, leading to a few centimeter thick gouge.

Compared to the hanging wall of the fault, in which fractures have been reopened thus facilitating water circulation (Gudmundsson, 2001), the footwall in which fractures remained tightly closed has been relatively preserved from weathering. We suggest that the dihedral fracture geometry, first described by Sevin (2014), well exposed in cap N'Dua cliffs (Fig. 3B) and in most mining sites, is a major control for horizontal water circulation within the saprock (Jeanpert, 2017) and depending upon the flow direction of the main aquifer, is responsible for lateral variation of Ni grade.

As shown by fracture analysis of cap N'Dua cliffs and drill-cores from 200 m depth in the Koniambo Massif (Jeanpert, 2017) (Fig. 1B), the fracture density does not vary significantly upward.

Therefore, in order to explain the downward limitation of surpergene orebodies, authors invoked the presence of listric faults (referred to as screen faults) (Leguéré, 1976; Genna et al., 2005; Sevin, 2014). However, these specific faults are not systematically observed within slope deposits and have never been described within plateau deposits. We argue that the classic *per descensum* model explain the vertical variation of permeability from the saprock horizon to the bedrock. Indeed, although the bedrock is highly fractured, fractures are sealed by serpentine and only reopen in sub-

surface allowing the development of the weathering profile. The very low permeability of the bedrock is sufficient to explain the downward limitation of Ni-rich waters.

Since the supergene reactivation of preexisting faults only happened in the upper part of peridotite massifs, with no equivalent in the autochthonous basement, and also because there are no modern equivalents of such large-scale slope failure, the elevation gradient cannot account alone for gravity-driven faulting. Therefore, fault reactivation was probably due to reduced frictional strength of preexisting faults provoked by increased water circulation on plateau edges under Late Oligocene and mid-Miocene wet climate (Zachos et al., 2001; Zachos et al., 2008) and intense rainfall periods.

In turn, 'supergene' gravity-driven slope collapse increased joint opening in the hanging wall of faults, enhanced rock permeability and hence favored weathering, which eventually resulted in an increase of Ni content in the saprock (Fig. 6 and Fig. 8). Meanwhile, symmetrical normal supergene faults, which display the same features and may be related to similar processes, appeared in the medial part of the massif. Edge collapse resulted in lateral decompression of the plateau and hence multi-directional extension (Fig. 8).

Conclusion

The early serpentinized fracture network plays a relevant role in supergene nickel ore forming processes. Due to the low permeability of peridotite bedrock, this network has been used during weathering by circulating meteoric waters. Field observations and DEM analysis show that this inherited network controlled incision of the pre-Miocene weathering surface and hence the plateau morphology of peridotite massifs. During a second stage of weathering, steep slopes, and water circulation in plateau edges were responsible for slope collapse, which in turn generated multidirectional extension in the massifs themselves. It resulted in increased joint opening and hence permeability, especially in the hanging wall of reactivated faults. Increased permeability enhanced weathering in highly fractured areas, thus forming mineralized burrows within plateaus and due to downward (i.e., centrifugal) circulation of the superficial water table, generated higher-grade slope deposits.

The very low permeability of unweathered peridotite of the bedrock cannot allow prominent water circulation and thus, the installation of a deep-seated hydrothermal system. Therefore, nickel-rich waters could not cross the bedrock, which never contains garnierite-like minerals. Instead, Ni-Mg silicate accumulation was restricted to open spaces (rock pores and open cracks) of the saprock; as a consequence, the heat source of low-temperature hydrothermal-like circulation was most probably located within the saprock itself.

Mining geologist currently use the serpentinization degree and geomorphology as guides for nickel exploration; in addition to that, we suggest that occurrence of zoned faults described in this paper signal the possible existence of slope and plateau deposits and can be used as an additional metallotect.

Acknowledgments

The authors warmly thank Willy Foucher (NMC), Pierre Rossler, Claire Montangerand, Clément Marcaillou, Pierre Epinoux and Aurélie Teaue (SLN), Maxime Drouillet (KNS), Cécile Fabre, Denis Fayard (SMGM) and Pascal Pico (Ballande) for giving access to the mining sites, thus enabling this study, and also for sharing their geological knowledge and field experience. The staff of the Geological Survey of New Caledonia is also thanked for welcome, helpful discussions, and support.

Moon V. and Proenza J.A. are thanked for throughout and constructive review of an early version of the ms.

This study is part of a PhD thesis co-funded by BRGM (French Geological Survey) and the University of New Caledonia. This article is a contribution of the 'CNRT Nickel and its environment' as a part of 'Ophiostruct' project (Geophysics and Structure of New Caledonia Ophiolite).

References

Aitchison, J.C., Clarke, G.L., Meffre, S., and Cluzel, D., 1995, Eocene arc-continent collision in New Caledonia and implications for regional southwest Pacific tectonic evolution: Geology, v. 23, no. 2, p. 161–164.

Andreani, M., 2003, Les microstructures de déformation des serpentines et la partition sismique-asismique: exemple de la Californie: Ph.D. thesis, France, Université de Grenoble I, 244 p.

Andreani, M., Grauby, O., Baronnet, A., and Muñoz, M., 2008, Occurrence, composition and growth of polyhedral serpentine: European Journal of Mineralogy, v. 20, no. 2, p. 159–171.

Andreani, M., Mével, C., Boullier, A.-M., and Escartin, J., 2007, Dynamic control on serpentine crystallization in veins: Constraints on hydration processes in oceanic peridotites: Geochemistry, Geophysics, Geosystems, v. 8, no. 2.

Avias, J., 1967, Overthrust structure of the main Ultrabasic New Caledonian massives: Tectonophysics, v. 4, no. 4–6, p. 531–541.

Avias, J., 1969, Note sur les facteurs contrôlant la genèse et la destruction des gîtes de nickel en Nouvelle-Calédonie. Importance des facteurs hydrologiques et hydrogéologiques.: Comptes Rendus de l'Académie des Sciences de Paris, v. 268, p. 244–246.

Avias, J., 1978, L'évolution des idées et des connaissances sur la genèse et sur la nature des minerais de nickel, en particulier latéritiques, de leur découverte à nos jours: Bulletin BRGM (Bureau des Recherches Géologiques et Minières), v. Section II, no. 3, p. 165–172.

Bailly, L., Ambrosi, J.P., Barbarand, J., Beauvais, A., Cluzel, D., Lerouge, C., Prognon, C., Quesnel, F., Ramanaïdou, E., Ruffet, G., Sevin, B., Wells, M., and Yans, J., 2014, Projet NICKAL: Typologie des latérites de Nouvelle-Calédonie et facteurs de concentration de Co et Ni: BRGM/RP-63482-FR, 402 p.

Bish, D.L., and Brindley, G.W., 1978, Deweylites, mixtures of poorly crystalline hydrous serpentine and talc-like minerals: Mineralogical Magazine, v. 42, p. 75–79.

Brand, N.W., Butt, C.R.M., and Elias, M., 1998, Nickel laterites: classification and features: Journal of Australian Geology & Geophysics, v. 17, no. 4, p. 81–88.

Butt, C.R.M., and Cluzel, D., 2013, Nickel laterite ore deposits: weathered serpentines: Elements, v. 9, p. 123–128.

Cathelineau, M., Myagkiy, A., Quesnel, B., Boiron, M.-C., Gautier, P., Boulvais, P., Ulrich, M., Truche, L., Golfier, F., and Drouillet, M., 2016a, Multistage crack seal vein and hydrothermal Ni enrichment in serpentinized ultramafic rocks (Koniambo massif, New Caledonia): Mineralium Deposita, p. 1–16.

Cathelineau, M., Quesnel, B., Gautier, P., Boulvais, P., Couteau, C., and Drouillet, M., 2016b, Nickel dispersion and enrichment at the bottom of the regolith: formation of pimelite target-like ores in rock block joints (Koniambo Ni deposit, New Caledonia): Mineralium Deposita, v. 51, no. 2, p. 271–282.

474 Chardon, D., Austin, J.A., Cabioch, G., Pelletier, B., Saustrup, S., and Sage, F., 2008, Neogene history
475 of the northeastern New Caledonia continental margin from multichannel reflection seismic
476 profiles: Comptes Rendus Geoscience, v. 340, no. 1, p. 68–73.

477 Chester, F., and Logan, J., 1986, Implications for mechanical properties of brittle faults from
478 observations of the Punchbowl fault zone, California: Pure and Applied Geophysics, v. 124,
479 no. 1–2, p. 79–106.

480 Chételat, E., 1947, La genèse et l'évolution des gisements de nickel de la Nouvelle-Calédonie: Bulletin
481 de la Société Géologique de France, v. 5, no. 1–3, p. 105–160.

482 Chevillotte, V., Chardon, D., Beauvais, A., Maurizot, P., and Colin, F., 2006, Long-term tropical
483 morphogenesis of New Caledonia (Southwest Pacific): Importance of positive epeirogeny and
484 climate change: Geomorphology, v. 81, no. 3–4, p. 361–375.

485 Cluzel, D., Aitchison, J.C., and Picard, C., 2001, Tectonic accretion and underplating of mafic terranes
486 in the Late Eocene intraoceanic fore-arc of New Caledonia (Southwest Pacific): geodynamic
487 implications: Tectonophysics, v. 340, p. 23–59.

488 Cluzel, D., Chiron, D., and Courme, M.-D., 1998, Discordance de l'Eocene superieur et évenements
489 pré-obduction en Nouvelle-Calédonie: Comptes Rendus de l'Académie des Sciences-Series
490 IIA-Earth and Planetary Science, v. 327, no. 7, p. 485–491.

491 Cluzel, D., Jourdan, F., Meffre, S., Maurizot, P., and Lesimple, S., 2012, The metamorphic sole of New
492 Caledonia ophiolite: ^{40} Ar/ ^{39} Ar, U-Pb, and geochemical evidence for subduction inception at
493 a spreading ridge: Tectonics, v. 31, no. 3.

494 Cluzel, D., and Vigier, B., 2008, Syntectonic mobility of supergene nickel ores of New Caledonia
495 (Southwest Pacific). Evidence from faulted regolith and garnierite veins: Resource Geology, v.
496 58, no. 2, p. 161–170.

497 Collot, J.Y., 1987, Overthrust emplacement of New Caledonia ophiolite: geophysical evidence:
498 Tectonics, v. 6, p. 215–232.

499 Coudray, J., 1976, Recherches sur le Néogène et le Quaternaire de la Nouvelle-Calédonie.
500 Contribution de l'étude sédimentologique à la connaissance de l'histoire géologique post-
501 Eocène de la Nouvelle-Calédonie: Expédition française sur les récifs coralliens de la Nouvelle-
502 Calédonie, v. 8, p. 183.

503 Deraisme, J., Bertoli, O., and Epinoux, P., 2014, Multivariate block simulations of a lateritic nickel
504 deposit and post-processing of a representative subset: Journal of the Southern African
505 Institute of Mining and Metallurgy, v. 114, no. 8, p. 673–680.

506 Dilek, Y., Coulton, A., and Hurst, S.D., 1997, Serpentinization and hydrothermal veining in peridotites
507 at site 920 in the Mark area: Proceedings-Ocean Drilling Program Scientific Results: National
508 Science Foundation, p. 35–60.

509 DTSI, 2013, Digital Elevation Model (10 m) - (Service de la Géomatique et de la Télédétection) -
510 Gouvernement de la Nouvelle-Calédonie.

511 Edwards, S.J., Schellart, W.P., and Duarte, J.C., 2015, Geodynamic models of continental subduction
512 and obduction of overriding plate forearc oceanic lithosphere on top of continental crust:
513 Tectonics, v. 34, no. 7, p. 1494–1515.

514 Eggleton, R.A., 2001, The regolith glossary: Cooperative Centre for Landscape Evolution and Mineral
515 Exploration, National Capital Printing: Canberra.

516 Evans, B.W., 2004, The Serpentinite Multisystem Revisited: Chrysotile Is Metastable: International
517 Geology Review, v. 46, no. 6, p. 479–506.

518 Evans, K.A., Powell, R., and Frost, B.R., 2013, Using equilibrium thermodynamics in the study of
519 metasomatic alteration, illustrated by an application to serpentinites: Lithos, v. 168–169, p.
520 67–84.

521 Freyssinet, P., 2005, Ore-forming processes related to lateritic weathering: Economic Geology, p.
522 681–722.

523 Fritsch, E., Juillot, F., Dublet, G., Fonteneau, L., Fandeur, D., Martin, E., Caner, L., Auzende, A.-L.,
524 Grauby, O., and Beaufort, D., 2016, An alternative model for the formation of hydrous Mg/Ni
525 layer silicates ('deweylite'/'garnierite') in faulted peridotites of New Caledonia: I. Texture and
526 mineralogy of a paragenetic succession of silicate infillings: European Journal of Mineralogy,
527 v. 28, no. 2, p. 295–311.

528 Frost, B.R., Evans, K.A., Swapp, S.M., Beard, J.S., and Mothersole, F.E., 2013, The process of
529 serpentinization in dunite from New Caledonia: Lithos, v. 178, p. 24–39.

530 Garnier, J., 1867, Note sur la geologie de la Nouvelle-Caledonie: Bulletin de la Société Géologique de
531 France, v. XXIV, no. 2, p. 438–451.

532 Gautier, P., Quesnel, B., Boulvais, P., and Cathelineau, M., 2016, The emplacement of the Peridotite
533 Nappe of New Caledonia and its bearing on the tectonics of obduction: Tectonics, v. 35, no.
534 12, p. 3070–3094.

535 Genna, A., Maurizot, P., Lafoy, Y., and Augé, T., 2005, Contrôle karstique de minéralisations
536 nickélifères de Nouvelle-Calédonie: Comptes Rendus Geoscience, v. 337, p. 367–374.

537 Golightly, J.P., 1981, Nickeliferous laterite deposits: Economic Geology, v. 75, p. 710–735.

538 Gudmundsson, A., 2001, Fluid overpressure and flow in fault zones: field measurements and models:
539 Tectonophysics, no. 336, p. 183–197.

540 Guillon, J.H., 1975, Les massifs péridotitiques de Nouvelle-Calédonie. Type d'appareil ultrabasique
541 stratiforme de chaîne récente: Mémoires ORSTOM, France, Paris, 120 p.

542 Guillot, S., Schwartz, S., Reynard, B., Agard, P., and Prigent, C., 2015, Tectonic significance of
543 serpentines: Tectonophysics, v. 646, p. 1–19.

544 Guillou-Frottier, L., Beauvais, A., Wyns, R., Bailly, L., Augé, T., and Audion, A.-S., 2015, Formation of
545 hydrothermal corrugations during weathering of ultramafic rocks, *in* Aquifères de Socle: le
546 Point sur les Concepts et les Applications Opérationnelles: Vingtièmes journées techniques
547 du Comité Français d'Hydrogéologie de l'Association Internationale des Hydrogéologues, La
548 Roche-sur-Yon, France, 2015, p. 8.

549 Hayes, D.E., and Ringis, J., 1973, Seafloor Spreading in the Tasman Sea: Nature, v. 244, p. 454–458.

550 Jeanpert, J., 2017, Structure et fonctionnement hydrogéologiques des massifs de péridotites de
551 Nouvelle-Calédonie: Université de la Réunion, Ph.D. thesis, 332 p.

552 Jeanpert, J., Genthon, P., Maurizot, P., Folio, J.-L., Vendé-Leclerc, M., Sérino, J., Join, J.-L., and Iseppi,
553 M., 2016, Morphology and distribution of dolines on ultramafic rocks from airborne LiDAR
554 data: The case of southern Grande Terre in New Caledonia (SW Pacific): Earth Surface
555 Processes and Landforms, v. 41, p. 1854–1868.

556 Jébrak, M., 1997, Hydrothermal breccias in vein-type ore deposits: a review of mechanisms,
557 morphology and size distribution: Ore geology reviews, v. 12, no. 3, p. 111–134.

558 Jébrak, M., and Marcoux, É., 2008, Géologie des ressources minérales: Ministère des ressources
559 naturelles et de la faune, 667 p.

560 Join, J.-L., Robineau, B., Ambrosi, J.-P., Costis, C., and Colin, F., 2005, Système hydrogéologique d'un
561 massif minier ultrabasique de Nouvelle-Calédonie: Comptes Rendus Geoscience, v. 337, no.
562 16, p. 1500–1508.

563 Kirkpatrick, J.D., Rowe, C.D., White, J.C., and Brodsky, E.E., 2013, Silica gel formation during fault slip:
564 Evidence from the rock record: Geology, v. 41, no. 9, p. 1015–1018.

565 Lagabrielle, Y., and Chauvet, A., 2008, The role of extensional tectonics in shaping Cenozoic New-
566 Caledonia: Bulletin de la Société Géologique de France, v. 179, no. 3, p. 315–329.

567 Lagabrielle, Y., Chauvet, A., Ulrich, M., and Guillot, S., 2013, Passive obduction and gravity-driven
568 emplacement of large ophiolitic sheets: The New Caledonia ophiolite (SW Pacific) as a case
569 study? Bulletin de la Société Géologique de France, v. 184, no. 6, p. 545–556.

570 Lagabrielle, Y., Maurizot, P., Lafoy, Y., Cabioch, G., Pelletier, B., Régnier, M., Wabete, I., and Calmant,
571 S., 2005, Post-Eocene extensional tectonics in Southern New Caledonia (SW Pacific): Insights
572 from onshore fault analysis and offshore seismic data: Tectonophysics, v. 403, no. 1–4, p. 1–
573 28.

574 Lahondère, D., Lesimple, S., Cagnard, F., Lahfid, A., Wille, G., and Maurizot, P., 2010, Serpentinisation
575 et fibrogenèse dans les massifs de péridotite de Nouvelle-Calédonie: BRGM/RP-60192-FR,
576 302 p.

577 Latham, M., 1986, Altération et pédogenèse sur roches ultrabasiques en Nouvelle-Calédonie; Genèse
578 et évolution des accumulations du fer et de silice en relation avec la formation du modelé:
579 Ph.D. thesis, France, Université de Dijon, 331 p.

580 Leguéré, J., 1976, Des corrélations entre la tectonique cassante et l'altération supergène des
581 péridotites de Nouvelle Calédonie: Ph.D. thesis, Université de Montpellier, 161 p.

582 Liversidge, A., 1880, Notes upon some minerals from New Caledonia: Thomas Richards, Government
583 Printer.

584 Maurizot, P., Cabioch, G., Fournier, F., Leonide, P., Sebih, S., Rouillard, P., Montaggioni, L., Collot, J.,
585 Martin-Garin, B., Chaproniere, G., Braga, J.C., and Sevin, B., 2016, Post-obduction carbonate

586 system development in New Caledonia (Népoui, Lower Miocene): Sedimentary Geology, v.
587 331, p. 42–62.

588 Maurizot, P., and Cluzel, D., 2014, Pre-obduction records of Eocene foreland basins in central New
589 Caledonia: an appraisal from surface geology and Cadart-1 borehole data: New Zealand
590 Journal of Geology and Geophysics, v. 57, no. 3, p. 300–311.

591 Maurizot, P., Sevin, B., Lesimple, S., Bailly, L., Iseppi, M., and Robineau, B., in press., Mineral
592 resources and prospectivity of the ultramafic rocks of New-Caledonia: Geology, geodynamics,
593 and mineral resources of New Caledonia: Ed. N. Mortimer Ch. 10 Memoir of the Geological
594 Society of London.

595 Maurizot, P., Sevin, B., Quesnel, F., and Wyns, R., 2014, Les sols et altérites comme ressources
596 minérales: Géosciences, no. 18, p. 70–79.

597 Maurizot, P., and Vendé-Leclerc, M., 2009, New Caledonia geological map, scale 1/500,000: Direction
598 de l'Industrie, des Mines et de l'Energie - Service de la Géologie de Nouvelle-Calédonie,
599 Bureau de Recherches Géologiques et Minières, Notice explicative par Maurizot P. et Collot,
600 J. (2009).

601 Milsom, J., 2003, Forearc ophiolites: A view from the western Pacific: Geological Society, London,
602 Special Publications, v. 218, no. 1, p. 507–515.

603 Moutte, J., and Paris, J.P., 1976, Anatomy and structure of the great southern massif (New
604 Caledonia): International Symposium on Geodynamics in South-West Pacific, Noumea, 1976,
605 p. 229–234.

606 Orloff, O., 1968, Etude géologique et géomorphologique des massifs d'ultrabasites compris entre
607 Houailou et Canala (Nouvelle-Calédonie): PhD Thesis, France, Université de Montpellier, 330
608 p.

609 Paquette, J.-L., and Cluzel, D., 2007, U–Pb zircon dating of post-obduction volcanic-arc granitoids and
610 a granulite-facies xenolith from New Caledonia. Inference on Southwest Pacific geodynamic
611 models: International Journal of Earth Sciences, v. 96, no. 4, p. 613–622.

612 Paris, J.-P., 1981, Géologie de la Nouvelle-Calédonie. Un essai de synthèse: Mémoire du B.R.G.M.,
613 278 p.

614 Peacock, D., Knipe, R., and Sanderson, D., 2000, Glossary of normal faults: Journal of Structural
615 Geology, v. 22, no. 3, p. 291–305.

616 Pelletier, B., 1996, Serpentines in nickel silicate ore from New Caledonia, *in* Nickel Conference –
617 Kalgoorlie, Western Australia, 1996, p. 197–205.

618 Prinzhofer, A., 1981, Structure et pétrologie d'un cortège ophiolitique: le massif du sud (Nouvelle
619 Calédonie). La transition manteau-croûte en milieu océanique: Ph.D. thesis, France, Paris,
620 Ecole Nationale Supérieure des Mines de Paris, 302 p.

621 Quesnel, B., 2015, Altération supergène, circulation des fluides et déformation interne du massif de
622 Koniambo, Nouvelle-Calédonie: implication sur les gisements nickélifères latéritiques: PhD
623 thesis, France, University of Rennes 1, 313 p.

624 Quesnel, B., Boulvais, P., Gautier, P., Cathelineau, M., John, C.M., Dierick, M., Agrinier, P., and
625 Drouillet, M., 2016, Paired stable isotopes (O, C) and clumped isotope thermometry of
626 magnesite and silica veins in the New Caledonia Peridotite Nappe: Geochimica et
627 Cosmochimica Acta, v. 183, p. 234–249.

628 Quesnel, B., Gautier, P., Boulvais, P., Cathelineau, M., Maurizot, P., Cluzel, D., Ulrich, M., Guillot, S.,
629 Lesimple, S., and Couteau, C., 2013, Syn-tectonic, meteorite water-derived carbonation of
630 the New Caledonia peridotite nappe: Geology, v. 41, no. 10, p. 1063–1066.

631 Quesnel, B., Gautier, P., Cathelineau, M., Boulvais, P., Couteau, C., and Drouillet, M., 2016b, The
632 internal deformation of the Peridotite Nappe of New Caledonia: A structural study of
633 serpentine-bearing faults and shear zones in the Koniambo Massif: Journal of Structural
634 Geology, v. 85, p. 51–67.

635 Quesnel, B., Le Carlier de Veslud, C., Boulvais, P., Gautier, P., Cathelineau, M., and Drouillet, M.,
636 2017, 3D modeling of the laterites on top of the Koniambo Massif, New Caledonia:
637 refinement of the per descensum lateritic model for nickel mineralization: Mineralium
638 Deposita, p. 1–18.

639 Robineau, B., Join, J.L., Beauvais, A., Parisot, J.-C., and Savin, C., 2007, Geoelectrical imaging of a thick
640 regolith developed on ultramafic rocks: groundwater influence: Australian Journal of Earth
641 Sciences, v. 54, no. 5, p. 773–781.

642 Roqué-Rosell, J., Villanova-de-Benavent, C., and Proenza, J.A., 2017, The accumulation of Ni in
643 serpentines and garnierites from the Falcondo Ni-laterite deposit (Dominican Republic)
644 elucidated by means of μXAS: Geochimica et Cosmochimica Acta, v. 198, p. 48–69.

645 Rouméjon, S., and Cannat, M., 2014, Serpentinization of mantle-derived peridotites at mid-ocean
646 ridges: Mesh texture development in the context of tectonic exhumation: Geochemistry,
647 Geophysics, Geosystems, v. 15, no. 6, p. 2354–2379.

648 Rouméjon, S., Cannat, M., Agrinier, P., Godard, M., and Andreani, M., 2015, Serpentinization and
649 fluid pathways in tectonically exhumed peridotites from the Southwest India ridge (62-65°E):
650 Journal of Petrology, v. 56, no. 4, p. 703–734.

651 Schwartz, S., Guillot, S., Reynard, B., Lafay, R., Debret, B., Nicollet, C., Lanari, P., and Auzende, A.L.,
652 2013, Pressure–temperature estimates of the lizardite/antigorite transition in high pressure
653 serpentinites: Lithos, v. 178, p. 197–210.

654 Sevin, B., 2014, Cartographie du régolithe sur formation ultrabasique de Nouvelle-Calédonie:
655 Localisation dans l'espace et le temps des gisements nickelifères: Ph.D. thesis, France,
656 Université de Nouvelle-Calédonie, 396 p.

657 Sevin, B., Cluzel, D., Maurizot, P., Ricordel-Prognon, C., Chaproniere, G., Folcher, N., and Quesnel, F.,
658 2014, A drastic lower Miocene regolith evolution triggered by post obduction slab break-off
659 and uplift in New Caledonia: Tectonics, v. 33, no. 9, p. 1787–1801.

660 Sevin, B., Ricordel-Prognon, C., Quesnel, F., Cluzel, D., Lesimple, S., and Maurizot, P., 2012, First
661 palaeomagnetic dating of ferricrete in New Caledonia: new insight on the morphogenesis
662 and palaeoweathering of "Grande Terre": First palaeomagnetic dating of ferricrete in New
663 Caledonia: Terra Nova, v. 24, no. 1, p. 77–85.

664 Sibson, R., 1977, Fault rocks and fault mechanisms: Journal of the Geological Society, v. 133, no. 3, p.
665 191–213.

666 Taylor, R.G., and Pollard, P.J., 1993, Mineralized Breccia Systems: Methods of Recognition and
667 Interpretation, 31 p.

668 Trescases, J.-J., 1973, L'évolution géochimique supergène des roches ultrabasiques en zone tropicale
669 et la formation des gisements nickélifères de Nouvelle-Calédonie: PhD thesis, France,
670 Université de Strasbourg, 379 p.

671 Troly, G., Esterle, M., Pelletier, B., and Reibell, W., 1979, Nickel deposits in New Caledonia, some
672 factors influencing their formation: International Laterite Symposium, New York, United
673 States, 1979, p. 85-119.

674 Trotet, F., Kadar, M., and Marini, D., 2015, Typology of the New Caledonian Ni-laterite deposits: from
675 natural to industrial processes: The Society for Geology Applied to Mineral Deposits, 13th
676 SGA meeting, Nancy, France, 4 p.

677 Ulrich, M., 2010, Péridotites et serpentinites du complexe ophiolitique de la Nouvelle-Caledonie.
678 Etudes pétrologiques, géochimiques et minéralogiques sur l'évolution d'une ophiolite de sa
679 formation à son altération: Ph.D. thesis, Université de la Nouvelle-Calédonie - Université
680 Joseph Fourier de Grenoble, 272 p.

681 Ulrich, M., Picard, C., Guillot, S., Chauvel, C., Cluzel, D., and Meffre, S., 2010, Multiple melting stages
682 and refertilization as indicators for ridge to subduction formation: The New Caledonia
683 ophiolite: Lithos, v. 115, p. 223–236.

684 U.S. Geological Survey, 2017, Mineral commodity summaries: Online, https://minerals.usgs.gov/
685 minerals /pubs /commodity /nickel /mcs-2017-nicke.pdf,.

686 Wirthmann, A., 1965, Die Reliefentwicklung von Neukaledonien: Deutscher Geog. Boch, p. 323–335.

687 Zachos, J.C., Dickens, G.R., and Zeebe, R.E., 2008, An early Cenozoic perspective on greenhouse
688 warming and carbon-cycle dynamics: Nature, v. 451, no. 7176, p. 279–283.

689 Zachos, J., Pagani, M., Sloan, L., Thomas, E., and Billups, K., 2001, Trends, Rhythms, and Aberrations
690 in Global Climate 65 Ma to Present: Science, v. 292, no. 5517, p. 686–693.

691

692 **Figure captions**

693 Fig. 1. A) Present-day tectonic configuration of the SW Pacific showing the distribution of major
694 tectonic features. Abbreviations: 3KR, Three Kings Ridge; CFZ, Cook Fracture Zone; LB, Loyalty Basin;
695 LHR, Lord Howe Rise; NC, New Caledonia; NLNZ, Northland New Zealand; NR, Norfolk Ridge; VMFZ,
696 Veining Meisnez Fracture Zone. B) Simplified geological map of New Caledonia showing the location
697 of the studied zones discussed in the text (after Maurizot and Vendé (2009).
698
699 Fig. 2. Typical weathering profile over ultramafic rocks of New Caledonia. Nomenclature after
700 Eggleton (2001) and Deraisme et al. (2014). Nickel content per horizons according to Jebrack and
701 Marcoux (2008).
702
703 Fig. 3. A) Lower hemisphere, equal area projection of the measured serpentinized fault network
704 positioned on a simplified geological map of the Cap n'Dua area. B) Photograph of the Cap n'Dua
705 cliffs and drawing from picture, highlighting the dihedral geometry of the fracture network in
706 unweathered peridotite.
707
708 Fig. 4. A) Geological map of the Kopéto Massif and lineaments interpreted from the Digital Terrain
709 Model (10 m) (DTSI, 2013) and stereonets showing the orientation of the serpentine-filled fractures
710 (straight green lines) compared to those filled with supergene minerals (black dashed lines). B)
711 Stereonets showing the orientations of i) serpentine-filled fractures (on the left), ii) supergene
712 mineralization reusing serpentine-filled fractures (grey straight lines), and iii) neoformed supergene
713 fractures(black dashed lines) in Vieille Carrière open-pit, located in Figure 3A.
714
715 Fig. 5. Normal fault in the Trafalgar exploration site in the northern side of Boulinda massif (Fig. 1B).
716 A) Simplified geological map of the studied area and interpreted lineaments. B) Aerial photograph of
717 the slump mass of the Trafalagar exploration site. C) Zonation of the fault zone associated to
718 detachment scarp. The hanging wall shows open joints filled with supergene silica and is more
719 weathered than the footwall. D) Zoom in the fault core zone. The fault gouge displays a 'ball-bearing'
720 breccia over a 20 cm thick cataclasite reusing a serpentine fault.
721
722 Fig. 6. Sketch of supergene fault zoning with zooms on the A) cataclasite of the footwall, B) the fault
723 gouge and C) the collapse breccia of the hanging wall.
724

Fig. 7. A) Main deweylite-coated fault controlling the pit of Vieille Carrière in the Kopéto massif and B) garnierite fault observed in the Yaté area (localization in Fig. 1B). These faults display the same zonation as Trafalgar fault (Fig. 5). C) Thin section of collapse breccia of the hanging wall of a supergene fault of Opoué mine site (Fig. 1B), the white arrow in upper right corner indicates the line of slope (see description in text). D) Hydraulic breccia within a joint of the hanging wall of the main deweylite fault of 'Vieille Carrière' pit (Fig. 7A).

Fig. 8. Simplified model of gravity-driven faulting in peridotite massifs and its significance for supergene nickel mineralization. Circulating meteoric water reduced the frictional strength, and together with the steep elevation gradient, provoked slope collapse. Meanwhile, normal faults marked by supergene breccia appeared in the inner parts of the massif. In turn, the increasing fracture density in the hanging walls of these faults enhanced permeability and hence favored weathering and eventually nickel concentration.

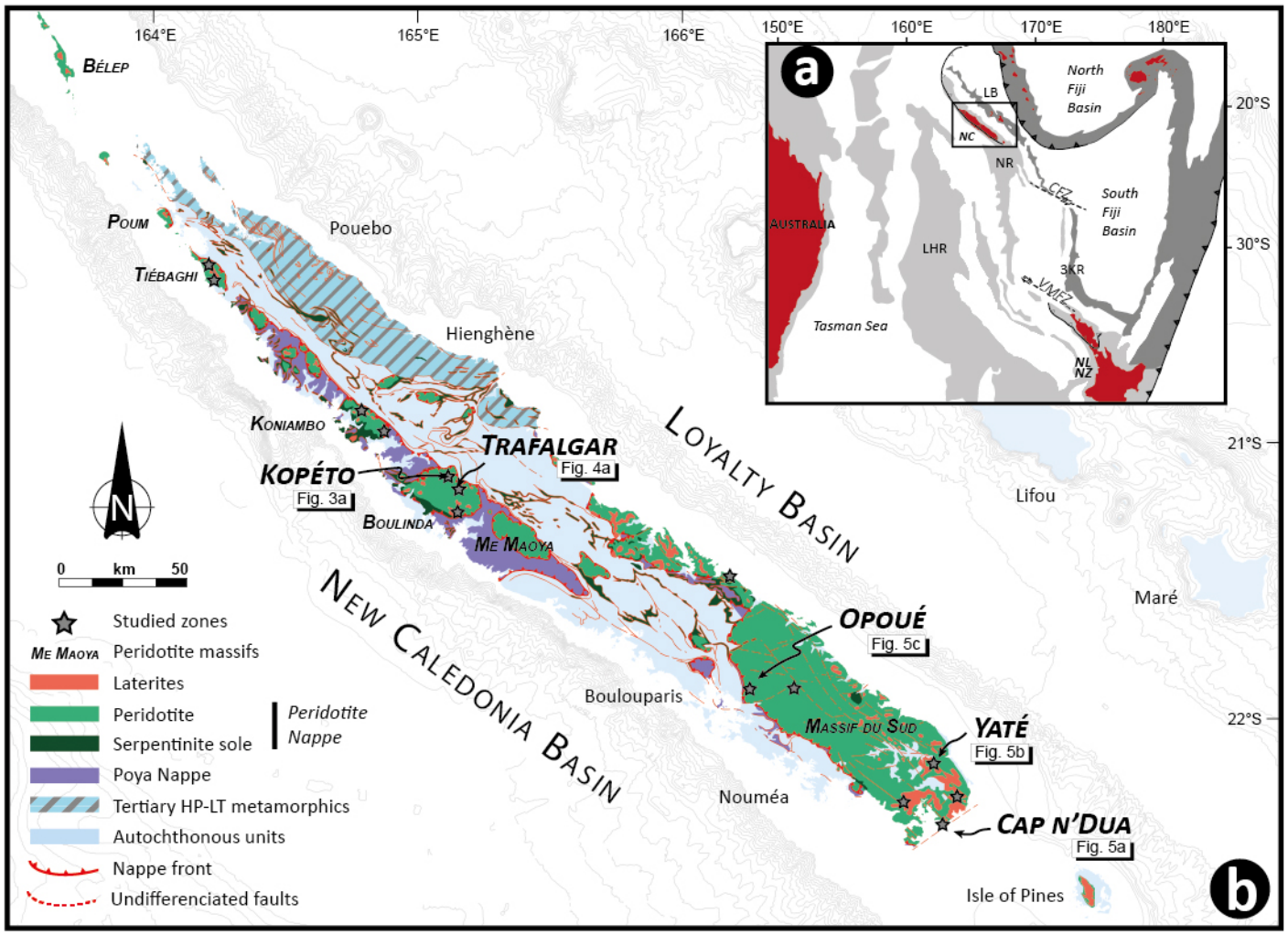
164°E
165°E
166°E
150°E
160°E
170°E
180°E
20°S
30°S
21°S
22°S
a
b
North Fiji Basin
South Fiji Basin
LB
NC
NR
CFZ
AUSTRALIA
LHR
3KR
VMFZ
Tasman Sea
NL
NZ
Bélep
Poum
Tiébaghi
Pouebo
Hienghène
Koniambo
Trafalgar
Fig. 4a
Kopéto
Fig. 3a
Boulinda
Me Maoya
Loyalty Basin
New Caledonia Basin
Lifou
Maré
Opoué
Fig. 5c
Boulouparis
Massif du Sud
Yaté
Fig. 5b
Nouméa
Cap N'Dua
Fig. 5a
Isle of Pines
N
0 km 50
Studied zones
Me Maoya Peridotite massifs
Laterites
Peridotite
Serpentinite sole
Peridotite Nappe
Poya Nappe
Tertiary HP-LT metamorphics
Autochthonous units
Nappe front
Undifferenciated faults

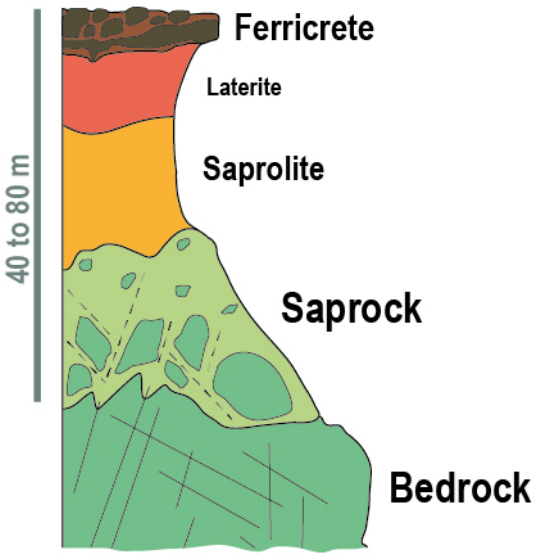
Ferricrete
Laterite
Saprolite
Saprock
Bedrock
40 to 80 m

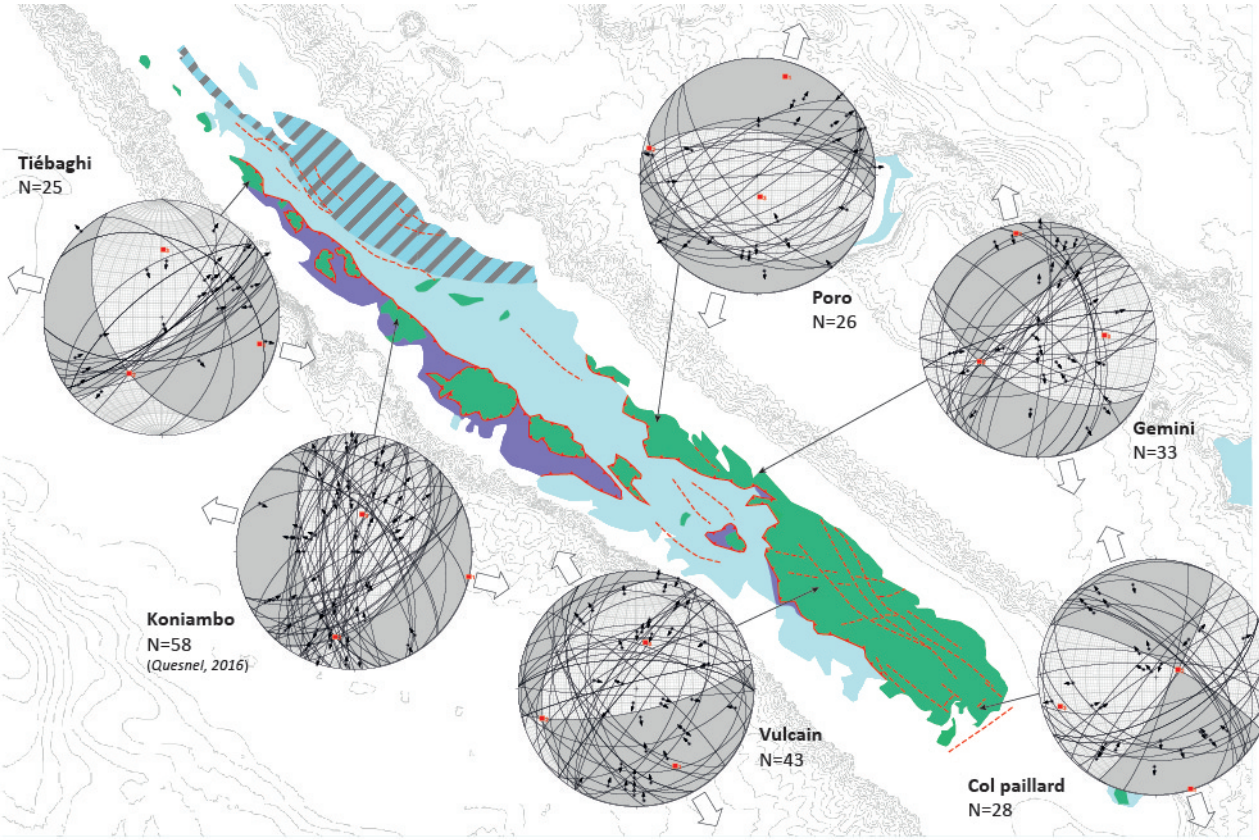
Tiébaghi
N=25
Poro
N=26
Gemini
N=33
Koniambo
N=58
(Quesnel, 2016)
Vulcain
N=43
Col paillard
N=28

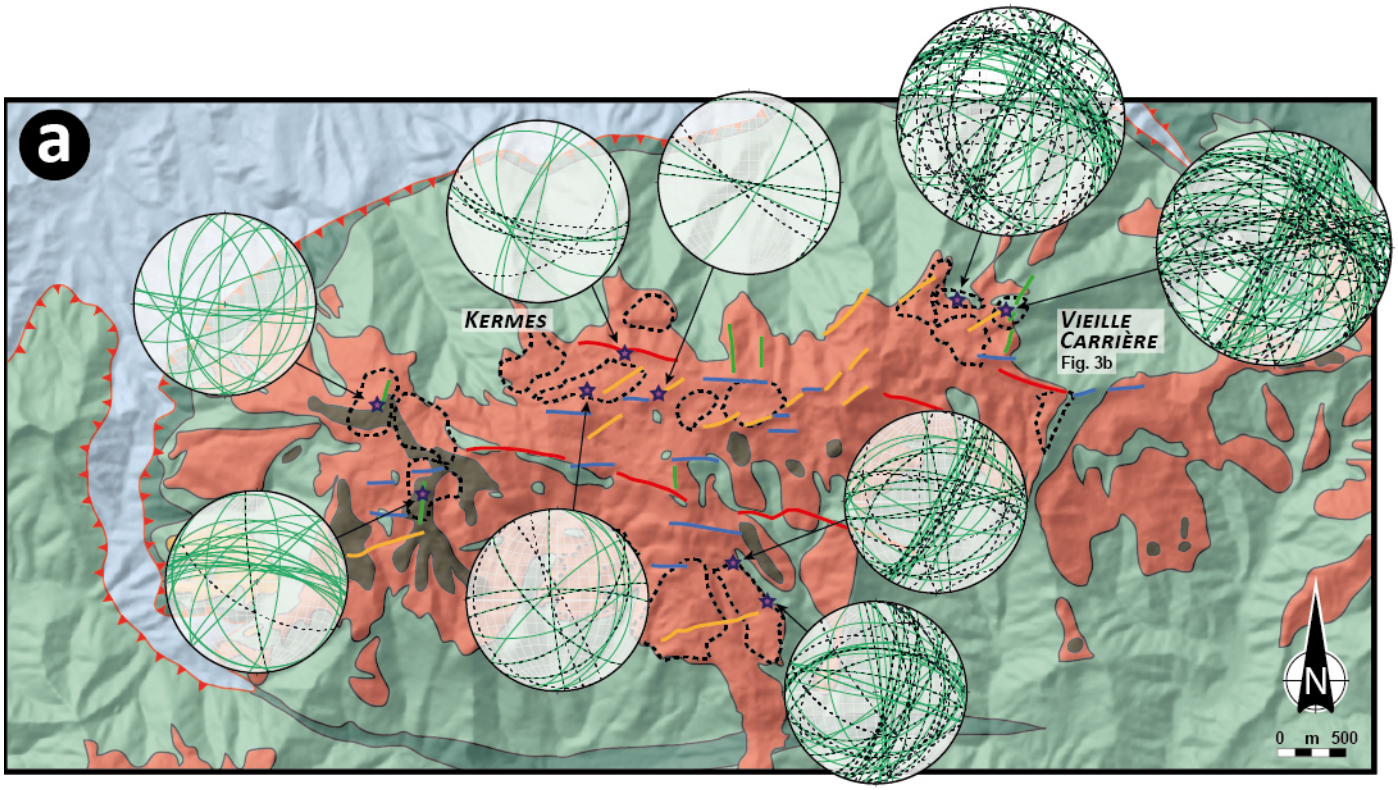
a
KERMES
VIEILLE CARRIÈRE
Fig. 3b
N
0 m 500
Geological map
Ferricrete
Laterite/Saprock
Peridotite
Serpentinite
Basal contact of the nappe
Volcano-sedimentary substratum
Interpreted lineaments family
N010°E lineaments
N050°E lineaments
N090°E lineaments
N130°E lineaments
Studied areas
Exploitation
Stereodiagrams
Serpentine fracture
Supergene fracture using a serpentine fracture
Neoformed supergene fracture

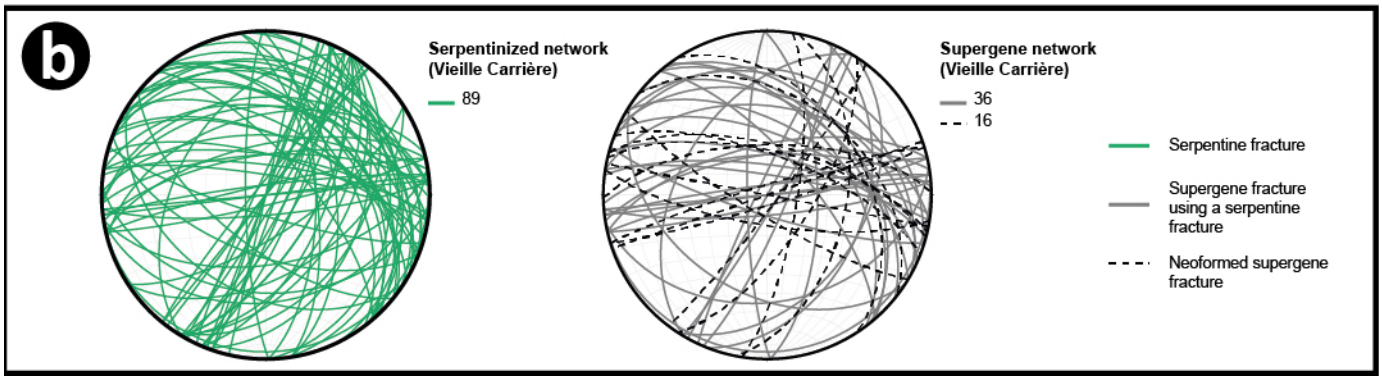
b
Serpentinized network
(Vieille Carrière)
89
Supergene network
(Vieille Carrière)
36
16
Serpentine fracture
Supergene fracture using a serpentine fracture
Neoformed supergene fracture

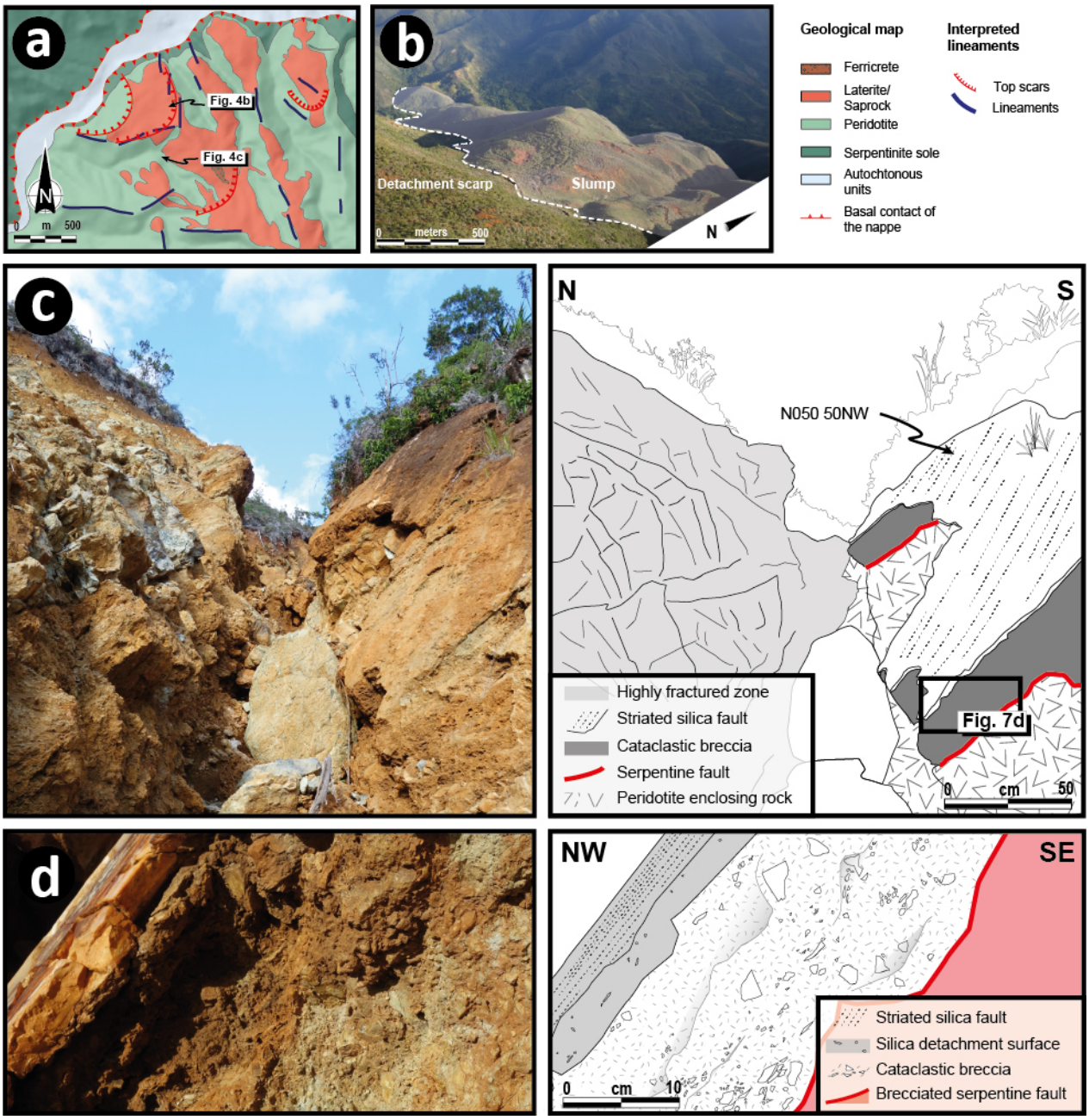
a
Fig. 4b
Fig. 4c
N
0 m 500
b
Detachment scarp
Slump
0 meters 500
N
Geological map
Ferricrete
Laterite/ Saprock
Peridotite
Serpentinite sole
Autochtonous units
Basal contact of the nappe
Interpreted lineaments
Top scars
Lineaments
c
N
S
N050 50NW
Highly fractured zone
Striated silica fault
Cataclastic breccia
Serpentine fault
Peridotite enclosing rock
Fig. 7d
0 cm 50
d
NW
SE
Striated silica fault
Silica detachment surface
Cataclastic breccia
Brecciated serpentine fault
0 cm 10

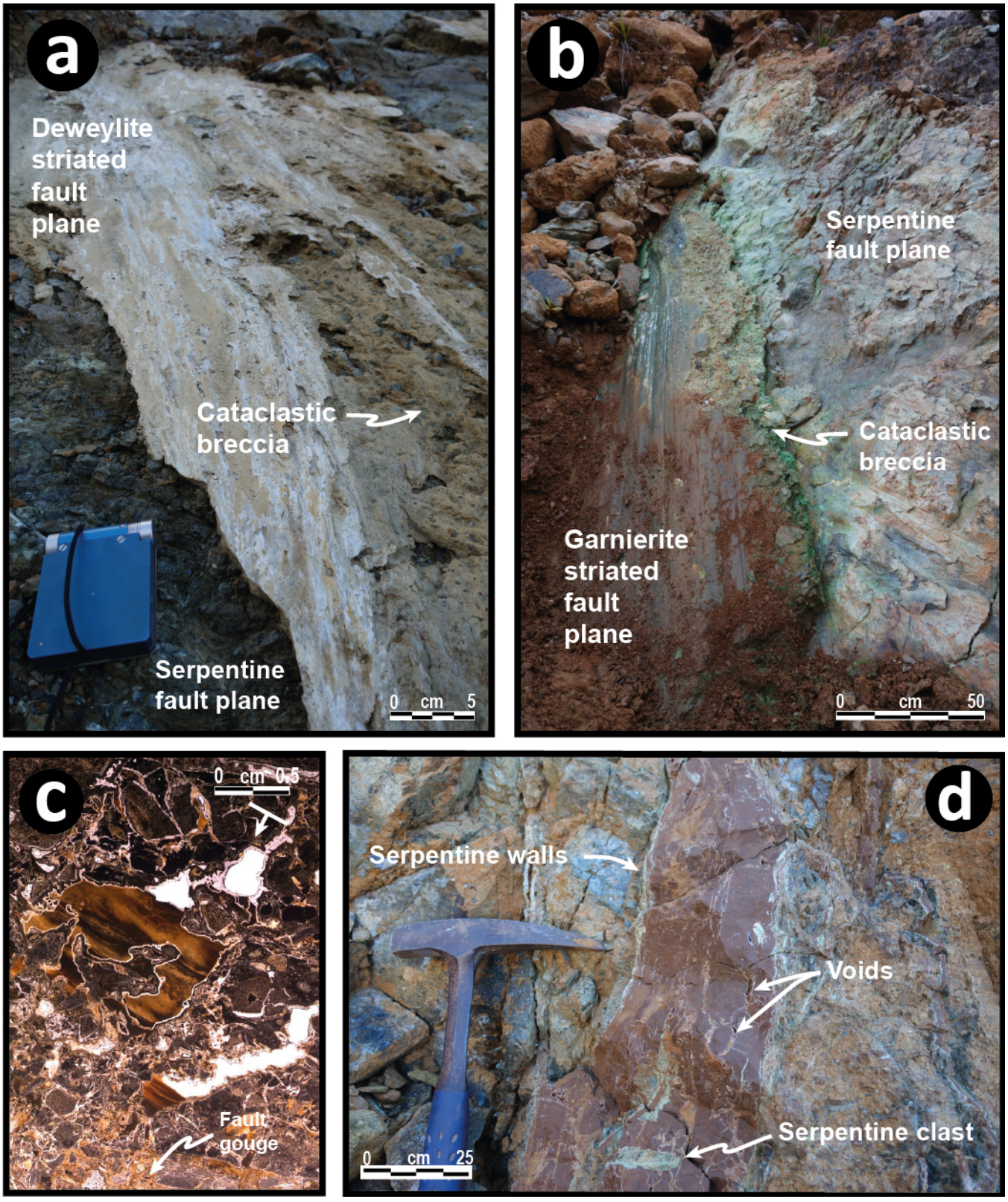
a
Deweylite striated fault plane
Cataclastic breccia
Serpentine fault plane
0 cm 5
b
Serpentine fault plane
Cataclastic breccia
Garnierite striated fault plane
0 cm 50
c
0 cm 0.5
Fault gouge
d
Serpentine walls
Voids
Serpentine clast
0 cm 25

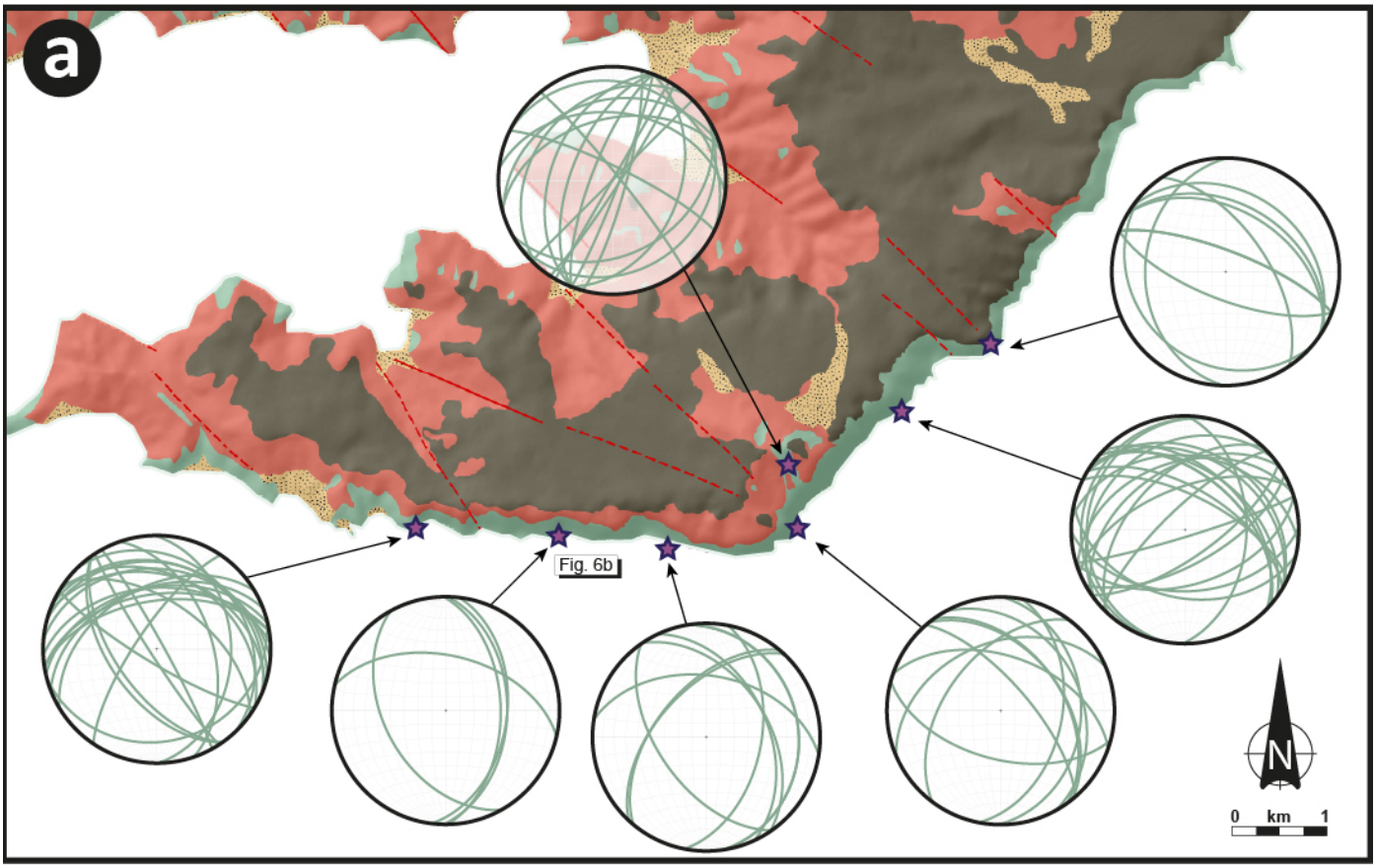

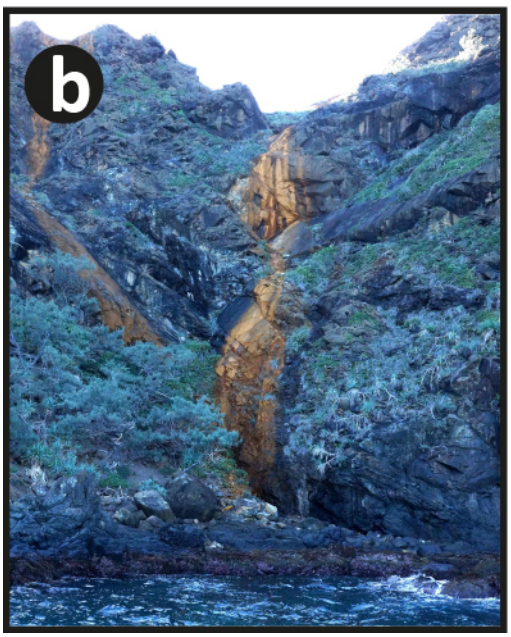

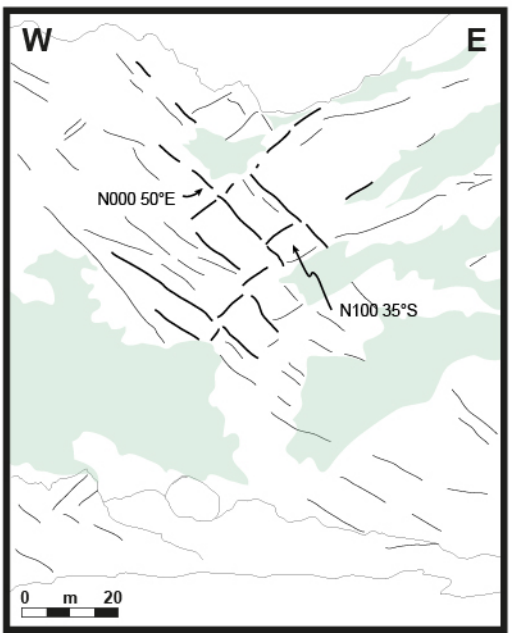

Geological map

- Alluvium
- Ferricrete
- Laterite/Saprock
- Peridotite
- Observed faults
- Supposed faults
- Observation points

Stereodiagrams

- Serpentine fracture

Photo interpretation

- Vegetation
- Dihedral geometry

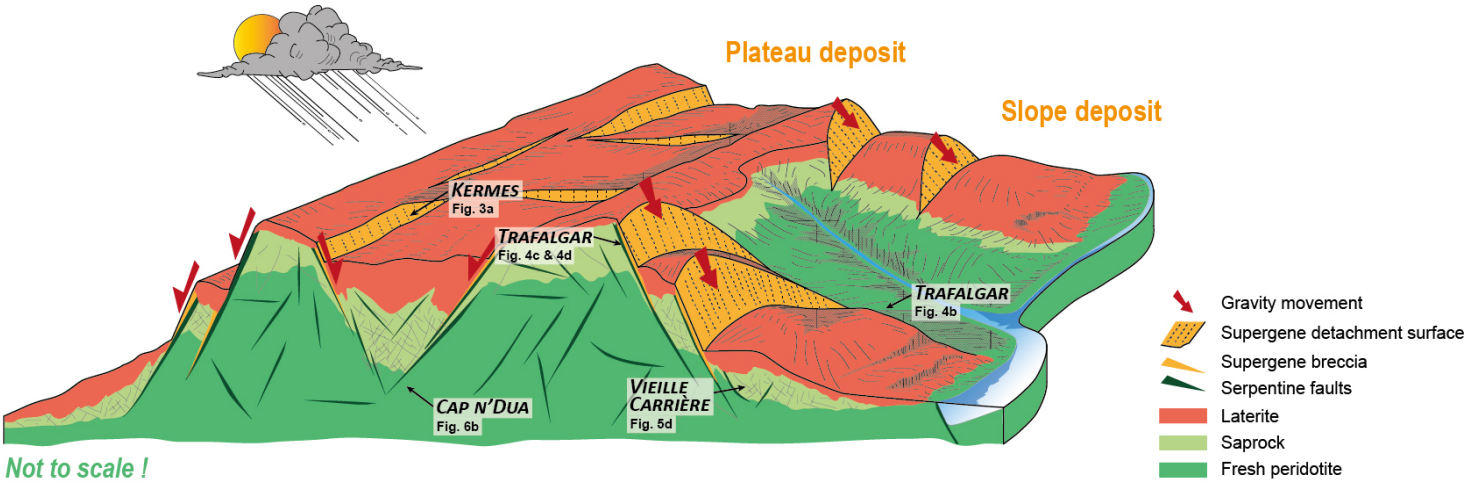
Plateau deposit
Slope deposit
KERMES
Fig. 3a
TRAFALGAR
Fig. 4c & 4d
TRAFALGAR
Fig. 4b
CAP N'DUA
Fig. 6b
VIEILLE CARRIÈRE
Fig. 5d
Not to scale !
Gravity movement
Supergene detachment surface
Supergene breccia
Serpentine faults
Laterite
Saprock
Fresh peridotite